エシェロンミラーを用いた高スループットなテラヘルツ分光ラインイメージング

浅井　岳，秦　大樹，原田真太郎，笠井達基，嵐田雄介，片山郁文

High-throughput Terahertz Spectral Line Imaging using an Echelon Mirror†

Gaku ASAI, Daiki HATA, Shintaro HARADA, Tatsuki KASAI, Yusuke ARASHIDA and Ikufumi KATAYAMA

本研究では，エシェロンミラーを用いたシングルショットテラヘルツ（THz）分光法と位相オフセット電気光学検出を組み合わせることにより，広帯域スペクトル情報を高感度に取得するテラヘルツ分光ラインイメージングを提案する．計測用カメラの単一ラインから得られるテラヘルツ帯スペクトル情報に対して，約 40 dB の信号対雑音比が得られ，1.2 kV/cm のピーク電場強度で最大 2 THz の帯域を検出できることを確認した．ラインイメージングにおける空間分解能は，テラヘルツ波のスペクトル成分ごとに回折限界程度であることが確認されている．今回提案したテラヘルツ分光ラインイメージングシステムにおいてサンプルを高速にスキャンすることで，二糖類（ラクトース，スクロース）の錠剤の成分分析・イメージングや樹脂サンプル等の膜厚・形状計測が可能となり，高いスループットで分光イメージングが可能であることを示した．

This work demonstrates terahertz (THz) line imaging that acquires broadband spectral information by combining echelon-based single-shot THz spectroscopy with high-sensitivity phase-offset electrooptic detection. A signal-to-noise ratio of approximately 40 dB is obtained for a THz spectrum from a single line of a camera with a detection bandwidth of up to 2 THz at the peak electric-field strength of 1.2 kV/cm. The spatial resolution of the image is confirmed to be diffraction limited for each spectral component of the THz wave. We use the system to image sugar tablets (lactose, sucrose) and film thickness/shape measurement of resin samples through a shield by quickly scanning the sample, which illustrates the capacity of the proposed spectral line imaging system for high-throughput applications.

Key words テラヘルツ波，超高速分光，イメージング，非破壊検査，高感度検出
terahertz wave, ultrafast spectroscopy, imaging, non-destructive inspection, high sensitivity detection

1 Introduction

Terahertz (THz) imaging is one of the most important applications of THz science and technology. It can be used to map materials that are difficult to distinguish using other frequency regimes [1], [2]. The material properties that can be detected using THz imaging include polymorphisms of organic materials [3], strain in rubbers [4], refractive indices of chemicals and proteins [5], [6], pigments in artificial paints [7], carriers in semiconductors [8], and foams in polymeric materials [9]. For these imaging applications, researchers have used THz cameras from microbolometers [10], THz CMOS cameras [11], and up-conversion to the near-infrared or visible range [12], etc. Although spectral information is fundamentally crucial for this technology, obtaining complete spectral information using these techniques is difficult and time-consuming.

An advanced technique for THz imaging is THz time-domain spectroscopy (THz-TDS), which uses ultrashort laser pulses and offers an important advantage over competing techniques [13], [14]. Because THz-TDS acquires the full temporal waveform of the THz transients, it can provide a precise broadband spectrum. However, increasing the measurement throughput is difficult because the temporal domain must be scanned to acquire the full waveform of the THz pulses, in addition to the spatial dimensions normally required for THz imaging.

Recently, significant efforts have been devoted to circumvent this difficulty by developing single-shot THz-TDS [15]–[17]. Yasui *et al.* used oblique crossings of THz waves and

† This paper was modified from reference [27] and added the result of thickness imaging of resin films as Fig. 5.

probe pulses in an electro-optic (EO) crystal to demonstrate single-shot THz line imaging [18]. However, the oblique-crossing technique requires a large EO crystal to map out sufficient temporal information; more importantly, the temporal information can be distorted by spatial inhomogeneities in the EO crystal and/or by scattered THz waves because different temporal information comes from different parts of the crystal.

The reflective echelon technique uses a stair-step mirror to map the temporal information to spatial positions on the mirror and allows us to focus the probe pulses on the EO crystal, which can reduce the distortion of the temporal waveforms [19], [20]. THz-TDS in a pulsed magnetic field and Kerr-gate spectroscopy have already been demonstrated using this method and have illustrated the precise acquisition of the temporal waveform and the corresponding spectrum [21]–[23]. In this study, we combine this technique based on an echelon mirror with a phase-offset method to enhance electric-field detection [24], and we implement the system in an imaging system to realize high-throughput line imaging.

2 Experiments

Fig. 1 summarizes the system used in this study. We used a Ti: sapphire regenerative amplifier with an output power of 1 mJ, center wavelength of 800 nm, and repetition rate of 1 kHz to generate and detect THz waves. Part of the laser output was used to pump the $LiNbO_3$ prism with a wavefront tilt to efficiently generate an intense THz wave [25], [26], which was subsequently collimated by using a spherical lens placed after the $LiNbO_3$ prism and linearly focused onto the sample with a cylindrical lens. Next, the THz image of the sample was transferred to the detection EO crystal, which detected the birefringence induced by the THz electric field and spatial distribution.

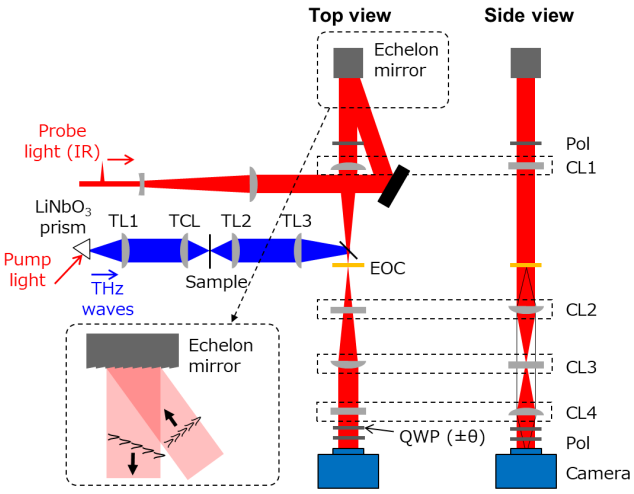

Fig. 1 Experimental setup for THz spectral line imaging using an echelon mirror. TL: THz Tsurupika lenses, TCL: THz cylindrical lens, CL: cylindrical lenses, EOC: electro-optic crystal, Pol: polarizers, QWP: quarter wave plate.

The remaining laser output of approximately 50 mW was used to probe the electric field distribution on the EO crystal, which was 1-mm-thick (110) ZnTe. The probe was reflected from an echelon mirror with a step width of 25 μm and step height of 2.5 μm, and linearly focused onto the crystal to cover the focal line of the THz wave. The number of steps on the echelon surface was 750. Because each segment of the echelon mirror reflects the probe pulse at different delay times (see inset of Fig. 1), the temporal information is mapped to the horizontal axis of the THz camera (16 bit, 2560 × 2160 pixels with a pixel size of 6.5 × 6.5 μm^2; full-well capacity of the camera was 30000 e-) upon imaging the echelon surface onto the camera. We used a set of cylindrical lenses after the EO crystal to image spatial information in the vertical direction. Using these setups, our system becomes scanless in THz spectral line imaging, which conventionally requires 2D scanning.

Because the THz pulses are linearly focused in our system, the electric field strength at the focus is less than that in other THz-TDS systems that use tightly focused THz pulses. To compensate for this reduced electric field strength, we enhanced the sensitivity of the EO sampling to obtain line imaging with a large signal-to-noise ratio (SNR). Here, we used the phase-offset method in the detection setup [24], and placed an EO crystal between the crossed polarizers and quarter wave plate with a slight offset rotation.

To describe the detection mechanism, we first write the Jones vector E_{in} of the incident probe pulse as:

$$E_{in} = \begin{pmatrix} E_x \\ E_y \end{pmatrix} = \begin{pmatrix} E_0 \\ 0 \end{pmatrix}. \quad (1)$$

The Jones matrix of modulated EO crystal is

$$J_{EO} = \begin{pmatrix} \cos\frac{\Delta}{2} & i\sin\frac{\Delta}{2} \\ i\sin\frac{\Delta}{2} & \cos\frac{\Delta}{2} \end{pmatrix}, \quad (2)$$

where Δ is the THz field-induced phase difference between the probe pulses. The Jones matrix of the offset quarter wave plate is

$$J_{\frac{\pi}{4}} = \begin{pmatrix} \cos\theta & -\sin\theta \\ \sin\theta & \cos\theta \end{pmatrix} \begin{pmatrix} e^{i\frac{\pi}{4}} & 0 \\ 0 & e^{-i\frac{\pi}{4}} \end{pmatrix} \begin{pmatrix} \cos\theta & \sin\theta \\ -\sin\theta & \cos\theta \end{pmatrix} = \frac{1}{\sqrt{2}} \begin{pmatrix} 1+i\cos 2\theta & i\sin 2\theta \\ i\sin 2\theta & 1-i\cos 2\theta \end{pmatrix}, \quad (3)$$

where θ is the angle of rotation in the 001 direction of the EO crystal. After the crossed analyzer polarizer, the output signal is

$$E_{\text{out}} = J_{\text{pol}} J_{\frac{\pi}{4}} J_{\text{EO}} E_{\text{in}} = \frac{E_0}{\sqrt{2}} \begin{pmatrix} 0 & 0 \\ 0 & 1 \end{pmatrix} \begin{pmatrix} 1+i\cos 2\theta & i\sin 2\theta \\ i\sin 2\theta & 1-i\cos 2\theta \end{pmatrix} \begin{pmatrix} \cos\frac{\Delta}{2} \\ i\sin\frac{\Delta}{2} \end{pmatrix} = \frac{E_0}{\sqrt{2}} \begin{pmatrix} 0 \\ i\sin 2\theta\cos\frac{\Delta}{2} + i\sin\frac{\Delta}{2} + \cos 2\theta\sin\frac{\Delta}{2} \end{pmatrix}. \quad (4)$$

The intensity of the signal is then

$$I(\theta,\Delta) = |E_{\text{out}}|^2 = \tfrac{1}{2}|E_0|^2 \left(\sin^2 2\theta\cos^2\tfrac{\Delta}{2} + \sin^2\tfrac{\Delta}{2} + \sin 2\theta\sin\Delta + \cos^2 2\theta\sin^2\tfrac{\Delta}{2}\right). \quad (5)$$

To eliminate the quadratic terms in this equation, we subtracted the data with the opposite phase offset to obtain

$$\frac{I(\theta,\Delta) - I(-\theta,\Delta)}{I(\theta,0)} = \frac{\Delta I}{I(\theta,0)} = \frac{2\sin\Delta}{\sin 2\theta}. \quad (6)$$

This equation ensures a one-to-one correspondence between the signal intensity and the electric field strength. Furthermore, enhancing the sensitivity of the measurement is possible by only changing the rotation angle θ of the QWP.

3 Results

Fig. 2(a) and 2(b) show the images obtained with the THz pulses at phase-offset angles of + 2° and −2°, respectively, with an exposure time of 50 ms. The images clearly show the THz pulses forming into a stripe pattern, with the two offset angles producing opposite polarities. Fig. 2(c) and 2(d) show the linear profiles taken along the 700th line of the images shown in Fig. 2(a) and 2(b), respectively, produced by calculating

$$\Delta I / I = (I_{\text{THzon}} - I_{\text{THzoff}}) / I_{\text{THzoff}}. \quad (7)$$

Using Eq. (6) to estimate the electric field, we subtracted the waveform with a negative phase offset from that with a positive phase offset to calculate the electric field strength, as shown in Fig. 2(e). Although the data were from a single line of the camera with no spatial averaging, the THz waveform obtained had a reasonable SNR.

Owing to the phase-offset method, we can use the full dynamic range of the camera for THz detection to enhance sensitivity. In contrast, if we use the QWP set at 45° for detection, as in the normal EO sampling method, we can use only 5% of the dynamic range, which results in a much worse SNR (typically 20 dB lower than SNR of the phase offset method if the THz electric field strength is similar to this work). Further enhancing the SNR may be possible if we simultaneously obtain signals with positive and negative phase offsets [16], [22]. The single-shot acquisition of an image can be demonstrated if we use a much higher power for the probe, although the data are not shown here.

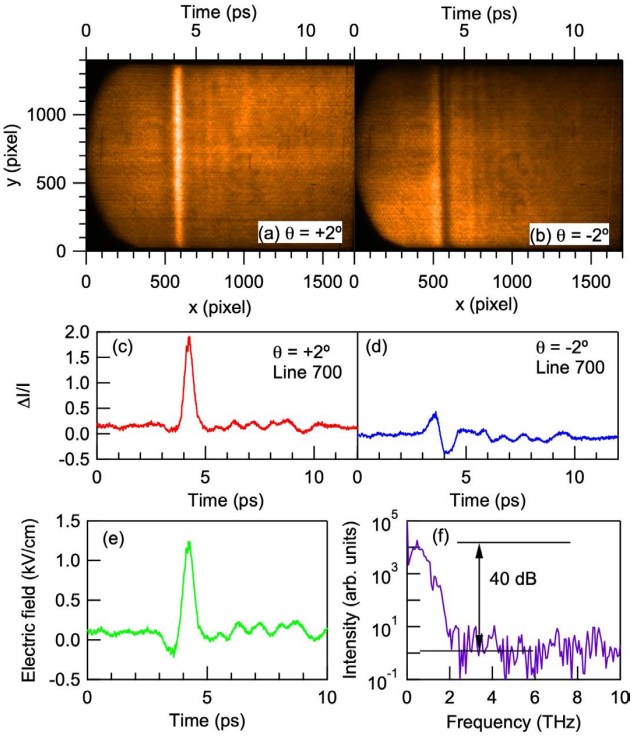

Fig. 2 THz spectral line imaging. Images taken with phase offset of (a) + 2° and (b) −2°. (c) and (d) are the vertical line profiles of the images shown in panels (a) and (b), respectively. (e) THz waveform obtained by subtracting the data of panel (d) from that of panel (c). (f) Fourier transform of panel (e).

Fig. 2(f) shows the Fourier transform of the line shown in Fig. 2(e). The spectrum of the THz wave clearly indicates that spectroscopy is possible for each pixel of the camera up to 2 THz. The SNR of this line reached 40 dB, which is very promising for THz line imaging with spectroscopic resolution. The SNR is determined primarily by the shot noise of the camera. The maximum count of the image can be set to approximately several 10000, which leads to an SNR of 100 for the electric field strength, and, thus, 40 dB for the intensity spectrum. Note that vertically averaging over several lines within the diffraction limit further increases the SNR. The results clearly demonstrate the possibility of enhancing

the throughput of THz imaging because we only need to scan one dimension (horizontal direction in our setup) to obtain full 2D information on the transmitted THz waveform at each point of the sample. The spectroscopic information acquired by this system allows us to both analyze materials with different characteristic THz absorptions and investigate the modifications of the spectrum in the THz range.

To demonstrate and characterize the imaging performance of the system, we measured the spatial resolution of the imaging system by blocking one part of the object plane with a metal plate. Fig. 3(a) shows a typical result of such an experiment, with the metal plate blocking part of the vertical extent of the image to characterize the spatial resolution in the vertical direction. In addition to the vertical lines that correspond to the incident THz pulses, we observed several non-vertical lines that originated from the edges of the metal plate. These correspond to THz pulse diffraction from the edge of the metal plate and the formation of interference patterns.

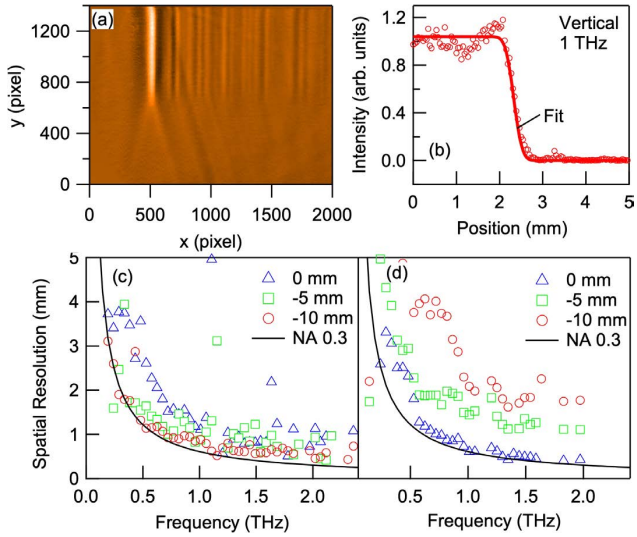

Fig. 3 (a) THz line image acquired with a metal plate blocking the bottom half of the object plane. (b) Vertical line profile of the measured THz wave at 1 THz. (c) Vertical and (d) horizontal spatial resolutions as a function of frequency estimated from the fitting shown in (b). Blue triangles, green rectangles, and red circles are the estimated spatial resolutions when the metal plate was placed just at the focus of the THz wave (0 mm), 5 mm, and 10 mm closer to the TCL, respectively. The solid line is the calculated spatial resolution considering the numerical aperture (0.3) of our setup.

The spatial resolution was estimated by fitting the vertical profile for each frequency component using the error function

$$I_0\{1+\mathrm{erf}[2\sqrt{\ln 2}(x-x_0)/d]\}/2, \quad (8)$$

as shown in Fig. 3(b), where x_0 is the central position of the THz wave, I_0 is the THz intensity, and d is the spatial resolution of the system. To characterize the horizontal resolution, we scanned the metal plate horizontally and examined the decrease in spectral intensity as a function of the position of the metal plate. The data were fitted to an error function to estimate the horizontal spatial resolution.

Fig. 3(c) and 3(d) show the vertical and horizontal spatial resolutions estimated from the width of the error function as a function of frequency. The black curve represents the diffraction limit of the system, calculated by assuming an estimated numerical aperture of 0.3. The data obtained with the metal plate not at the focal plane are also plotted. These results were consistent with those of the measured spatial resolution of the system, although the data for the vertical direction were slightly worse than those of the diffraction limit. This difference may be caused by a slight misalignment of the system, especially the focusing lens, before the sample. Because the imaging system was designed with spherical lenses, the spatial resolutions for the horizontal and vertical directions were the same, even though the sample was illuminated with a cylindrical lens.

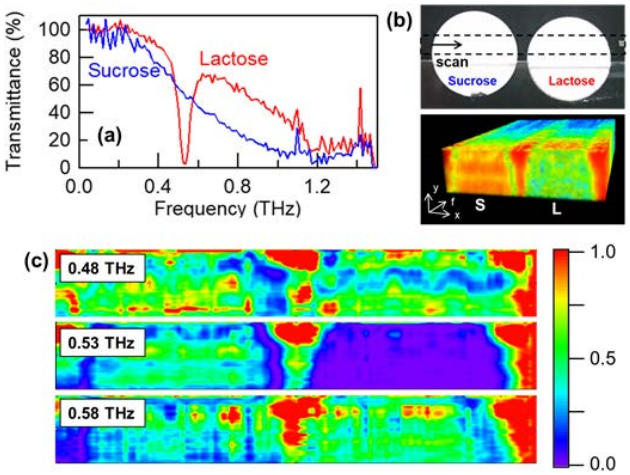

Fig. 4 (a) Transmittance spectra of the sucrose and lactose tablets. (b) Picture of the disaccharide tablets under investigation. The lower part shows the full spectral absorption image plotted in color for 3D. (c) Slices of the 3D transmittance data taken at indicated frequencies.

Next, to demonstrate spectral line imaging, we prepared two disaccharide tablets with different spectral characteristics in the THz region, as shown in Fig. 4(a). Lactose has a characteristic absorption at 0.53 THz, whereas sucrose only has a smooth absorption up to 1 THz. We scanned the sample shown in Fig. 4(b) in the horizontal direction, and data for a width of approximately 36 mm and height of approxi-

mately 5 mm were obtained. The vertical direction (y-axis) was imaged using the line-imaging system. The obtained full spectral imaging data plotted as a 3D image are shown in the lower part of Fig. 4(b). Fig. 4(c) shows the slices of the data at several frequencies: 0.48 THz, 0.53 THz, 0.58 THz. The data clearly show the difference in the absorption at 0.53 THz between two tablets where strong absorption of lactose exists.

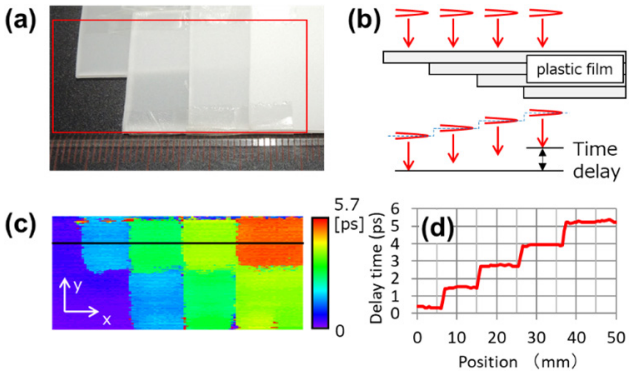

Fig. 5 (a) Picture of plastic film samples of different thickness (measurement range is in the red frame). (b) Conceptual diagram of the principle of thickness measurement. (c) Distribution of delay time transmitted through plastic film. (d) Cross-sectional graph on the black line.

Finally, to demonstrate the advantages of time-resolved spectroscopic imaging, an example of thickness imaging of a resin film that is opaque to visible light is presented. As shown in Fig. 5(a), samples with different numbers of films depending on the position were prepared and measured using the spectroscopic line-imaging system proposed in this paper. As shown in Fig. 5(b), the delay time $\tau(= nd/c)$ of the THz pulse changes depending on the thickness of the transmitted sample. Therefore, the film thickness is obtained by extracting the peak value of the time waveform acquired by time-domain spectroscopy (n: refractive index in the THz region, d: film thickness, c: speed of light). Fig. 5(c) shows a thickness map wherein the delay time is plotted for film samples of different thicknesses. Fig. 5(d) shows a cross-sectional graph on the black line (equivalent to an optical path length difference of 300 μm per 1 ps delay time).

These figures show that the step difference due to the change in the number of films is well represented. Using time-resolved spectroscopic imaging, the transmitted thickness imaging of a sample that is opaque to visible light was demonstrated and it was shown to be a promising means for measuring the 3D and film thickness of resins and ceramics in the future.

The results shown in Fig. 4 and Fig. 5 indicate that spectral line imaging using an echelon mirror is very promising for future industrial and scientific applications. A 3D color image of the sample is of essential importance for comparing and distinguishing materials with different THz responses. Using our imaging system, spectral information is obtained on a single-shot basis, which can avoid distorting the THz waveform due to temporal fluctuations, such as changes in the spectrum or position of the sample. Additionally, combining our system with a compressive sampling technique to expand the spatial dimensions of the imaging is possible. The full and reliable spectral information in the THz region obtainable in our system can be the key to realizing such applications in the future.

4 Conclusion

In summary, we demonstrated spectral line imaging by combining a single-shot THz detection technique using an echelon mirror with the phase offset method. The obtained SNR of the single line reached 40 dB, thereby offering a sufficient dynamic range for spectroscopy applications. The spatial resolutions in both the horizontal and vertical directions were comparable to the diffraction limit of the THz waves at each frequency component. The results obtained from the imaging of disaccharide tablets demonstrate the high potential of spectral line imaging for future applications.

References

[1] M. Tonouchi, "Cutting-edge terahertz technology," *Nat. Photonics*, vol. 1, no. 2, pp. 95–105, 2007.

[2] H. Guerboukha, K. Nallappan, and M. Skorobogatiy, "Toward real-time terahertz imaging," *Adv. Opt. Photonics*, vol. 10, no. 4, pp. 843–938, 2018.

[3] K. Ajito, Y. Ueno, H.-J. Song, E. Tamechika, and N. Kukutsu, "Terahertz Spectroscopic Imaging of Polymorphic Forms in Pharmaceutical Crystals," *Mol. Cryst. Liquid Cryst.*, vol. 539, no. 1, pp. 33–38, 2011.

[4] A. Moriwaki, M. Okano, and S. Watanabe, "Internal triaxial strain imaging of visibly opaque black rubbers with terahertz polarization spectroscopy," *APL Photonics*, vol. 2, no. 10, 106101, 2017.

[5] K. Kawase, Y. Ogawa, Y. Watanabe, and H. Inoue, "Non-destructive terahertz imaging of illicit drugs using spectral fingerprints," *Opt. Express*, vol. 11, no. 20, pp. 2549–2554, 2003.

[6] X. Han, S. Yan, Z. Zang, D. Wei, H. L. Cui, and C. Du, "Label-free protein detection using terahertz time-domain spectroscopy," *Biomed. Opt. Express*, vol. 9, no. 3, pp. 994–1005, 2018.

[7] K. Fukunaga, N. Sekine, I. Hosako, N. Oda, H. Yoneyama, and T. Sudou, "Real-time terahertz imaging for art conservation science," *J. Euro. Opt. Soc*., vol. 3, 08027, 2008.

[8] A. J. Huber, F. Keilmann, J. Wittborn, J. Aizpurua, and R. Hillenbrand, "Terahertz Near-Field Nanoscopy of Mobile Carriers in Single Semiconductor Nanodevices," *Nano Lett*., vol. 8, no. 11, pp. 3766–3770, 2008.

[9] D. J. Roth, S. Reyes-Rodriguez, D. A. Zimdars, R. W. Rauser, and W. W. Ussery, "Terahertz computed tomography of NASA thermal protection system materials," in *AIP Conf. Proc*., vol. 1430, p. 566, 2012.

[10] J. Oden, J. Meilhan, J. Lalanne-Dera, J.-F. Roux, F. Garet, J.-L. Coutaz, and F. Simoens, "Imaging of broadband terahertz beams using an array of antenna-coupled microbolometers operating at room temperature," *Opt. Express*, vol. 21, no. 4, pp. 4817–4825, 2013.

[11] F. Schuster, D. Coquillat, H. Videlier, M. Sakowicz, F. Teppe, L. Dussopt, B. Giffard, T. Skotnicki, and W. Knap, "Broadband terahertz imaging with highly sensitive silicon CMOS detectors," *Opt. Express*, vol. 19, no. 8, pp. 7827–7832, 2011.

[12] P. Bai, Y. Zhang, T. Wang, Z. Fu, D. Shao, Z. Li, W. Wan, H. Li, J. Cao, X. Guo, and W. Shen, "Broadband THz to NIR up-converter for photon-type THz imaging," *Nat. Commun*., vol. 10, no. 1, 3513, 2019.

[13] B. Ferguson and X.-C. Zhang, "Materials for terahertz science and technology," *Nat. Mater*., vol. 1, no. 1, pp. 26–33, 2002.

[14] T. Kampfrath, K. Tanaka, and K. A. Nelson, "Resonant and nonresonant control over matter and light by intense terahertz transients," *Nat. Photonics*, vol. 7, no. 9, pp. 680–690, 2013.

[15] Z. Jiang and X.-C. Zhang, "Electro-optic measurement of THz field pulses with a chirped optical beam," *Appl. Phys. Lett*., vol. 72, no. 16, pp. 1945–1947, 1998.

[16] S. M. Teo, B. K. Ofori-Okai, C. A. Werley, and K. A. Nelson, "Invited Article: Single-shot THz detection techniques optimized for multidimensional THz spectroscopy," *Rev. Sci. Instrum*., vol. 86, no. 5, 051301, 2015.

[17] Z.-H. Zhai, S.-C. Zhong, J. Li, L.-G. Zhu, K. Meng, J. Li, Q. Liu, Q.-X. Peng, Z.-R. Li, and J.-H. Zhao, "Time-resolved single-shot terahertz time-domain spectroscopy for ultrafast irreversible processes," *Rev. Sci. Instrum*., vol. 87, no. 9, 095101, 2016.

[18] T. Yasui, K.-I. Sawanaka, A. Ihara, E. Abraham, M. Hashimoto, and T. Araki, "Real-time terahertz color scanner for moving objects," *Opt. Express*, vol. 16, no. 2, pp. 1208–1221, 2008.

[19] Y. Minami, Y. Hayashi, J. Takeda, and I. Katayama, "Single-shot measurement of a terahertz electric-field waveform using a reflective echelon mirror," *Appl. Phys. Lett*., vol. 103, no. 5, 051103, 2013.

[20] I. Katayama, H. Sakaibara, and J. Takeda, "Real-Time Time-Frequency Imaging of Ultrashort Laser Pulses Using an Echelon Mirror," *Jpn. J. Appl. Phys*., vol. 50, no. 10, 102701, 2011.

[21] X. Li, K. Yoshioka, M. Xie, G. T. Noe, W. Lee, N. Marquez Peraca, W. Gao, T. Hagiwara, O. S. Handegard, L.-W. Nien, T. Nagao, M. Kitajima, H. Nojiri, C.-K. Shih, A. H. MacDonald, I. Katayama, J. Takeda, G. A. Fiete, and J. Kono, "Terahertz Faraday and Kerr rotation spectroscopy of BiI-xSbx films in high magnetic fields up to 30 tesla," *Phys. Rev. B*, vol. 100, no. 11, 115145, 2019.

[22] G. T. Noe, I. Katayama, F. Katsutani, J. J. Allred, J. A. Horowitz, D. M. Sullivan, Q. Zhang, F. Sekiguchi, G. L. Woods, M. C. Hoffmann, H. Nojiri, J. Takeda, and J. Kono, "Single-shot terahertz time-domain spectroscopy in pulsed high magnetic fields," *Opt. Express*, vol. 24, no. 26, pp. 30328–30337, 2016.

[23] G. Mead, I. Katayama, J. Takeda, and G. A. Blake, "An echelon-based single shot optical and terahertz Kerr effect spectrometer," *Rev. Sci. Instrum*., vol. 90, no. 5, 053107, 2019.

[24] J. Degert, M. Cornet, E. Abraham, and E. Freysz, "Simple and distortion-free optical sampling of terahertz pulses via heterodyne detection schemes," *J. Opt. Soc. Am. B*, vol. 33, no. 10, pp. 2045–2050, 2016.

[25] J. Hebling, G. Almasi, I. Z. Kozma, and J. Kuhl, "Velocity matching by pulse front tilting for large-area THz-pulse generation," *Opt. Express*, vol. 10, no. 21, pp. 1161–1166, 2002.

[26] H. Hirori, A. Doi, F. Blanchard, and K. Tanaka, "Single-cycle terahertz pulses with amplitudes exceeding 1 MV/cm generated by optical rectification in $LiNbO_3$," *Appl. Phys. Lett*., vol. 98, no. 9, 091106, 2011.

[27] G. Asai, D. Hata, S. Harada, T. Kasai, Y. Arashida and I. Katayama, "High-throughput terahertz spectral line imaging using an echelon mirror," *Opt. Express*, vol. 29, no. 3, pp. 3515–3522, 2021.

浅井　岳　Gaku ASAI
光学本部 要素開発部
Fundamental Technology Development Department
Optical Engineering Division

秦　大樹　Daiki HATA
光学本部 要素開発部
Fundamental Technology Development Department
Optical Engineering Division

原田真太郎　Shintaro HARADA
横浜国立大学
Yokohama National University

笠井達基　Tatsuki KASAI
横浜国立大学
Yokohama National University

嵐田雄介　Yusuke ARASHIDA
筑波大学
University of Tsukuba

片山郁文　Ikufumi KATAYAMA
横浜国立大学
Yokohama National University


浅井　岳
Gaku ASAI


秦　大樹
Daiki HATA


原田真太郎
Shintaro HARADA


笠井達基
Tatsuki KASAI


嵐田雄介
Yusuke ARASHIDA


片山郁文
Ikufumi KATAYAMA